Three-Dimensional Fluid Model for Atmospheric Pressure Dielectric Barrier Discharge Plasma

Muhammad M. Iqbal,* Miles M. Turner

We developed a three-dimensional fluid model to investigate the evolution of filamentation during the breakdown phase in an atmospheric pressure DBD plasma. Filamentation is a major source of instability in DBD plasma and it develops frequently under distinct conditions. In this study, we explore the dynamic behavior of filaments under the influence of overvoltage and driving frequency. The filamentary profile of atmospheric pressure dielectric barrier discharge is suppressed in the breakdown phase when the frequency varies in the specified domain (2.5–25 kHz) in He-N_2 gas mixture. In particular, we contrast the spatial profiles of discharge parameters in the case of uniform and non-uniform discharge plasma. The trapping mechanism of electrons is identified only at higher frequencies (>50 kHz) than small frequencies in the uniform DBD plasma. This simulation study describes the importance of three-dimensional modeling for the understanding of the filamentary and uniform discharge plasmas in the breakdown phase.

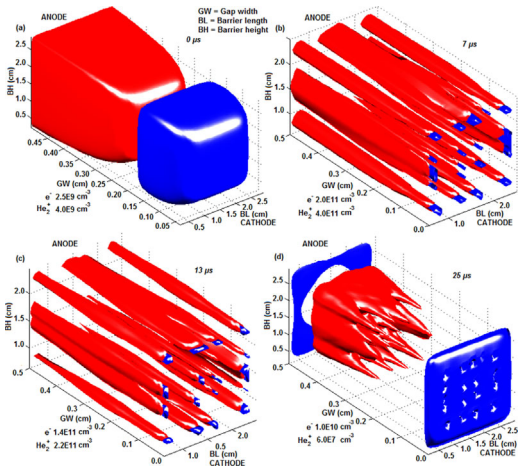

1. Introduction

Recently, the atmospheric pressure dielectric barrier discharges have been recognized as extremely attractive and beneficial in many branches of industry, such as large scale of ozone generation, surface polymerization, exhaust gas treatment, plasma using spray droplets, sterilization of cavities and surfaces, biology, medicines, pollution control, deposition of thin film for distinct types of applications.[1–7] The instability caused by filamentation in dielectric barrier discharge plasma frequently exists at atmospheric pressure and is not necessarily required because of their adverse effects in many applications of discharge plasma. There are several studies in literature that investigated the behavior of uniformity in atmospheric pressure dielectric barrier discharge (DBD) plasmas using experimental as well as numerical modeling techniques.[8–11] The elementary explanation of discharge plasma can be possible by employing one-dimensional models that ignore the expansion and dynamic interaction of discharge species in other directions. The two-dimensional models describe significantly improved insight for the structure of discharge species of plasma in the radial and axial directions, but still lack of realistic illustration of plasma process,[12–15] which is only achievable with a three-dimensional modeling approach. In addition, the role of computational modeling is identified as an essential component for expressing of plasma processes[16] in more

Dr. M. M. Iqbal, M. M. Turner
National Centre for Plasma Science and Technology, Dublin City University, Glasnevin, Dublin 9, Ireland
E-mail: muhammad.iqbal3@mail.dcu.ie

Plasma Process. Polym. **2015,** DOI: 10.1002/ppap.201400231
© 2015 WILEY-VCH Verlag GmbH & Co. KGaA, Weinheim

Early View Publication; these are NOT the final page numbers, use DOI for citation !!

detail under strict operating conditions. Three-dimensional numerical modeling methods have been perceived as essential to reveal the important features and dynamic aspects of discharge plasma, indicating the emphasis of numerical simulations for the characterization of weakly ionized plasmas.

The behavior and pattern formation of non-uniformities as filaments and streamers were analyzed by using the multi-dimensional numerical models in distinct gas mixtures with various kinds of reactor geometries under a wide range of working conditions[17–20]; however, the precise behavior of the filaments in the DBD plasma stills requires better understanding in three-dimensional space. In DBD plasma, the physical description of the plasma properties at atmospheric pressure have been explained by considering the role of parameters, such as relative permittivity, width of dielectric barrier, gap spacing, and the quantity of trace impurities in inert gas.[10,12,21] The accumulation or eradication of surface charge density (SCD) depends on the polarity reversal of external imposed oscillating sinusoidal potential. The significance of the breakdown mechanism of discharge plasma has been investigated from the initial and subsequent cycles in detail that explained the pattern formation and dynamics of plasma filaments in dielectric barrier discharges at high pressure in various gas mixtures, such as helium, neon, and nitrogen under various imposed operating constraints.[22] The breakdown potential of a gas mixture is reduced by introducing Penning impurities (N_2 and O_2) in the gas that diminishes the value of breakdown voltage[14,21,23] in discharge plasma.

In this simulation study, we have considered the influence of overvoltage as well as the higher recombination coefficient (RC) of molecular nitrogen ions in the lower domain of frequency (5–25 kHz), which are actually employed to develop a feasible environment for the evolution of filamentation in the streamer breakdown phase. It is significantly important to introduce a proper amount of nitrogen impurities in the helium gas for the development of uniform glow discharge plasma because the nitrogen impurities are performed as a destructive agent for the metastables through the sharp channel of Penning ionization. The different quantities of nitrogen impurities (20–50 ppm) are introduced in the higher domain (30–90 kHz) and the above-mentioned lower domain of frequency to examine the dynamic characteristics of the uniform glow and filamentary atmospheric pressure DBD plasma. In the higher domain of frequency, the trapping mechanism of electrons is observed specifically near the anode barrier at the peak of the discharge current density and in particular, this feature is going to be contrasted at different frequencies. These observations provide a clear motivation of dividing the domain of driving frequency into two parts. A self-consistent uniform atmospheric pressure DBD plasma is obtained under the influence of external imposed potential as 1.5 kV because it is slightly greater than the breakdown potential at the gap spacing of 0.5 cm. The magnitude of external imposed potential is enhanced to 1.7 kV to explore the influential behavior of filamentation in the breakdown phase. The stationary-state is acquired in both cases of uniform and filamentary DBD plasmas to describe the authenticity of numerical simulations. The average number of cycles is 5–6 in the case of small domain of frequency, while the number of cycles becomes double in the higher domain of frequency.

2. Fluid Model Formulation

2.1. Fluid Model Equations and Schematic Geometry

In the rectangular simulation domain, the oscillating sinusoidal potential ($V_0 \sin(2\pi ft)$) is imposed to the driven electrode at a particular frequency (f) and the other electrode is grounded, where V_0 is the amplitude of sinusoidal potential as shown in Figure 1. The barrier width (BW) is smaller than the gap spacing (GW) between the dielectric barriers, but the barrier width is different in various sections of this paper. The discharge is ignited in the open rectangular area after the breakdown of gas mixture near the surface of dielectric barriers alternatively during the positive and negative discharge current pulses. The stagnant mixture of He-N_2 gas is considered for the numerical simulations throughout this study. We consider first three moments of the Boltzmann equation[16] in this numerical modeling study, which provides the conservation of moments of participating discharge species. Let us take a three-dimensional planar rectangular coordinate system of the parallel plate dielectric barrier discharge geometry under an impact of oscillating sinusoidal

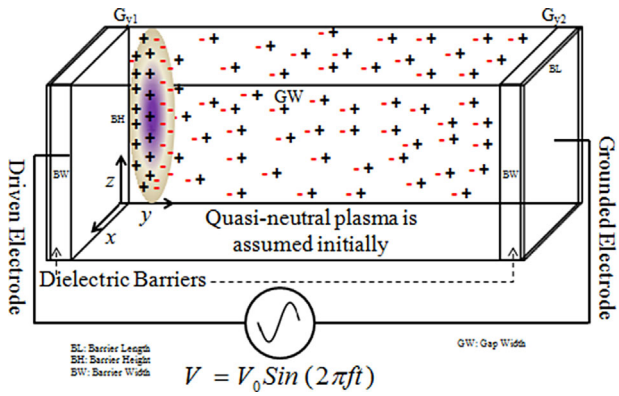

Figure 1. Symbolic representation of parallel plate dielectric barrier discharge geometry under the application of oscillating sinusoidal potential.

© 2015 WILEY-VCH Verlag GmbH & Co. KGaA, Weinheim
DOI: 10.1002/ppap.201400231

Early View Publication; these are NOT the final page numbers, use DOI for citation !!

potential. The density profiles of discharge interacting species (e^-, He^+, He_2^+, N_2^+, He^*, and He_2^*) are estimated by considering a particle balance equation as

$$\frac{\partial n_{sp}(x,y,z,t)}{\partial t} + \vec{\nabla}.\vec{\Gamma}_{sp}(x,y,z,t) = S_{sp} \quad (1)$$

where n_{sp}, $\vec{\Gamma}_{sp} = \mathrm{sgn}(q_{sp})\mu_{sp}\vec{E}\,n_{sp} - D_{sp}\vec{\nabla}\,n_{sp}$, and S_{sp} represent the species density, drift-diffusion flux, and source term for the production and annihilation of discharge species as mentioned in Table 1,[13] q_{sp} is the charge on discharge species, D_{sp} is the diffusion coefficient. To include the contribution of electrons in the discharge plasma, the electron mean energy ($\bar{\epsilon}$) is determined by using the electron energy density balance equation as

$$\frac{\partial n_\varepsilon(x,y,z,t)}{\partial t} + \vec{\nabla}.\vec{\Gamma}_\varepsilon(x,y,z,t) = S_\varepsilon \quad (2)$$

where $n_\epsilon(x,y,z,t) = n_e(x,y,z,t)\bar{\epsilon}(x,y,z,t)$ is the electron energy density, n_e is the electron density, and $\vec{\Gamma}_\varepsilon = -(5/3)\mu_e\vec{E}\,n_\varepsilon - (5/3)D_e\vec{\nabla}\,n_\varepsilon$ is the drift-diffusion flux in the electron energy density equation. The source term S_ϵ (x, y, z, t) can be calculated as

$$S_\epsilon = \underbrace{-\vec{\Gamma}_\epsilon.\vec{E}}_{\mathrm{I}} \underbrace{-n_e\sum_k \epsilon_k k_k n_k}_{\mathrm{II}} \underbrace{-\xi^k(n_\epsilon^{k+1} - n_e^{k+1}\bar{\epsilon}^k)}_{\mathrm{III}} \quad (3)$$

Here the first term (I) on RHS of Eq. (3) is the Joule heating created by the electric field and the second term (II) is the electron energy losses due to the elastic and inelastic collisions, respectively. The third term (III) represents an implicit correction of the energy source term for the variations in the electron mean energy, which quenches oscillations in the numerical solution of the electron energy density equation, and the further details of this term are available in ref.[24] In order to evaluate the electric field of discharge plasma, the Poisson's equation is coupled with the plasma fluid model for the estimation of electric field. For the estimation of electric potential, the Poisson's equation for the electric potential (V) can be represented as

$$\vec{\nabla}.(\varepsilon_0\vec{\nabla}\,V) = \sum_{sp} q_{sp}n_{sp} \quad (4)$$

where ϵ_0 is the permittivity of free space and the electric field strengths ($\vec{E}$) are calculated from the gradient of the electric potential along x, y, and z directions as $E_x = -\partial V/\partial x$, $E_y = -\partial V/\partial y$, and $E_z = -\partial V/\partial z$. The local field approximation (LFA) applies to the ionic species in which the transport and reaction rate coefficients are dependent on the electric field. In order to consider the inertial effects of ions at high pressure, the effective electric field (E_{sp}^{eff})[25] is calculated for the transport of ions in discharge plasma as

$$\frac{\partial \vec{E}_{sp}^{eff}}{\partial t} = \nu_{eff}(\vec{E} - \vec{E}_{sp}^{eff}) \quad (5)$$

where $\nu_{eff} = q_i/(\mu_i m_i)$ is the effective ion-neutral collision frequency, q_i is the charge on the ionic species, μ_i is the mobility of ions, and m_i is the corresponding mass of ionic species. The flux of discharge species is evaluated at the boundaries by the following set of equations:

$$\begin{aligned}
\vec{\Gamma}_{sp}.\hat{n} &= (2\beta-1)\mathrm{sgn}(q_{sp})\mu_{sp}\vec{E}_{sp}^{eff}.\hat{n}n_{sp} + \frac{1}{2}v_{th,sp}n_{sp}\\
\vec{\Gamma}_e.\hat{n} &= -(2\beta-1)\mu_e\vec{E}.\hat{n}n_e + \frac{1}{2}v_{th,e}n_e - 2(1-\beta)\sum_{sp}\gamma_{sp}\vec{\Gamma}_{sp}.\hat{n}\\
\vec{\Gamma}_\epsilon.\hat{n} &= -(2\beta-1)\frac{5}{3}\mu_e\vec{E}.\hat{n}n_\epsilon(x,y,z,t) + \frac{2}{3}v_{th,e}n_\epsilon(x,y,z,t)\\
\vec{\Gamma}_n.\hat{n} &= \frac{1}{2}v_{th,n}n_n(x,y,z,t)
\end{aligned} \quad (6)$$

where it represents the boundary conditions for the parallel plate dielectric barriers and $\hat{n}$ is the normal vector pointing toward the dielectric barriers, $v_{th,sp} = \sqrt{8k_BT_{sp}/\pi m_{sp}}$ is the thermal velocity of discharge species, k_B is the Boltzmann constant, T_{sp} is the gas species temperature, and m_{sp} is the particle species mass. The thermal velocity ($v_{th,sp}$) of discharge species of gas is determined at room temperature in this modeling study. The integer number (β) is set to 1 if the drift velocity is directed toward the dielectric barriers and to 0 otherwise

$$\beta = \begin{cases} 1 & sgn(q)\mu\vec{E}.\hat{n} > 0 \\ 0 & sgn(q)\mu\vec{E}.\hat{n} \le 0 \end{cases} \quad (7)$$

For open boundaries, the gradient of following discharge variables vanishes. Therefore, the discharge species density, electron energy density, and electrical potential at (x, z) = 0 and (x, z) = (L, H) can be expressed as

$$\begin{aligned}
&\frac{\partial n_{sp}(0,y,z,t)}{\partial x} = 0, \frac{\partial n_{sp}(x,y,0,t)}{\partial z} = 0,\\
&\frac{\partial n_{sp}(L,y,z,t)}{\partial x} = 0, \frac{\partial n_{sp}(x,y,H,t)}{\partial z} = 0
\end{aligned} \quad (8)$$

Table 1. Maximum values of species density at various frequencies at $V_o = -1.7$ kV, $\epsilon_r = 9.0$, and 50 ppm N_2 impurities.

Driving frequency [kHz]	Electron density $[cm^{-3}] \times 10^{11}$	He_2^+ ion density $[cm^{-3}] \times 10^{11}$
2.5	2.51	5.02
5	2.33	4.50
10	2.02	4.03
15	0.80	1.50
20	0.62	1.21
25	0.31	0.62

© 2015 WILEY-VCH Verlag GmbH & Co. KGaA, Weinheim

Early View Publication; these are NOT the final page numbers, use DOI for citation !!

where sp = e, i, n, $\bar{\epsilon}$ and V illustrates the electrons, ions, neutrals (metastables and excimers), electron mean energy, and electric potential. The symbols L and H represent the maximum length and height of the plasma reactor along the x and z directions. So the purpose of dielectric barrier is to accumulate charges during the breakdown operation of the atmospheric pressure DBD and it is evaluated by using Gauss's law[10] as

$$-\epsilon_0\frac{\partial V}{\partial y}(G^+_{y1},x,y,z,t)+\epsilon_0\epsilon_r\frac{\partial V}{\partial y}(G^-_{y1},x,y,z)=\sigma_s(G_{y1},x,y,z,t)$$
$$+\epsilon_0\frac{\partial V}{\partial y}(G^-_{y2},x,y,z,t)-\epsilon_0\epsilon_r\frac{\partial V}{\partial y}(G^+_{y2},x,y,z)=\sigma_s(G_{y2},x,y,z,t) \quad (9)$$

where σ_s is the SCD and ϵ_r is the relative permittivity of dielectric barrier, $G^{\pm}_{y1,y2}$ corresponds to the boundary edge cells on both sides of dielectric barriers and, the superscripts '+' and '−' correspond to advancing the boundary from the positive and negative y-direction, respectively as shown in Figure 1.

2.2. Transport and Discharge Operating Properties

To provide the details of operating conditions of the parallel plate DBD geometry, a mixture of He-N_2 gas is considered at a constant pressure of 760 Torr and room temperature as 300 K. The varying amount of nitrogen impurities, such as 20 and 50 ppm is supplied in the pure helium gas for different case studies and the secondary electron emission coefficient (γ_p) is taken as 0.01[21] for the ionic species. The length (L) and height (H) of DBD reactor are supposed as 3.0 cm. The gap spacing between the dielectric barriers is assumed as 0.5 cm to be constant throughout this investigation. The mobility of electrons as well as reaction rate coefficients of direct ionization and excitation chemical processes are determined by using the freeware Boltzmann solver BOLSIG+.[26] The reduced diffusion coefficients and mobilities of ionic species (He^+, He_2^+, and N_2^+) in the He-N_2 gas mixture are calculated from the data available in ref.[27] and some references cited therein. The diffusion coefficients of the neutral species are similar as used in ref.[13] for the He-N_2 gas mixture. The chemistry of He-N_2 gas mixture is based on the chemical reaction scheme as described in ref.[28] since the significance of the RC of N_2^+ ions has been described in ref.[14] using a two-dimensional fluid model.

We discussed the impact of higher RC in the case of filamentary discharge plasma because its influence emerges only in the afterglow phase. It eradicates the seed electrons before the next breakdown of DBD plasma. The reduction of the electron density in the pre-breakdown phase forms an appropriate medium for the development of filamentary discharge plasma. The higher value of RC of molecular nitrogen ions is used in Figures 2–4, while the standard reference value of RC[13] is utilized for Figures 5 and 6. The quasi-neutral plasma is assumed before the start of numerical simulations and the initial density of electrons and ions is $\sim 10^9$ cm^{-3} for different cases in this study. The simulations presented here deal with a three-dimensional fluid model for He-N_2 DBD plasma implemented on a single user desktop workstation using a time step $\sim 10^{-10}$ s, which provides a description of filamentary and uniform atmospheric pressure discharge plasma in the breakdown phase using He-N_2 gas mixture. The mesh independence is obtained to provide the reliability of numerical simulations and the minimum number of mesh points are considered as (34, 34, 34) along the x, y, and z directions that are in accordance with ref.[32] The uniform mesh is used in this simulation and the smallest values of parameters between the grid cells are ($\Delta x = 0.0882$, $\Delta y = 0.0147$, and $\Delta z = 0.0882$ cm).

2.3. Strategy for numerical solution

The finite difference method (FDM) is considered as adequate to discretize the system of three-dimensional fluid model equations, while the Courant-Friedrichs-Levy condition $\Delta t < \left(\epsilon_o/\sum_p |q_p|\mu_p n_p\right)$ is implemented to evaluate the value of minimum time step for the numerical simulations[29] in order to avoid artificial instabilities. The Scharfetter-Gummel exponential scheme[30] is employed for the discretization of transport terms in the continuity equations of discharge species and the electron energy density equation. The three-dimensional system of plasma fluid model equations is numerically solved by using a semi-implicit sequential iterative scheme with uniform grid that provides a flexibility to enhance the time step by many orders of magnitude, hence, allowing a rapid evaluation of numerical simulations. The particle balance equations for discharge species are transformed into sets of linear seven-point equations, which are solved by employing MSI solver as explained in ref.[31,32] A convergence criterion ($||R|| < 10^{-4}$ ($||A|| + ||A_c||\ ||U||$)) is implemented for the evaluation of iterative solution using MSI solver, where $||R||$ represents the norm, A and A_c are the coefficients of the matrix (U) in linearized format. In case of Poisson's equation, the successive over relaxation (SOR) method[33] is implemented in which the overrelaxation parameter (ω) lies in the interval ($1.5 < \omega < 2.0$) for rapid convergence. As the electron energy density involves the implicit correction term (III) in Eq. (3), the alternating direction implicit (ADI) procedure[34] is considered as efficient to solve the energy density equation, which provides the numerical solution in

© 2015 WILEY-VCH Verlag GmbH & Co. KGaA, Weinheim

Early View Publication; these are NOT the final page numbers, use DOI for citation !!

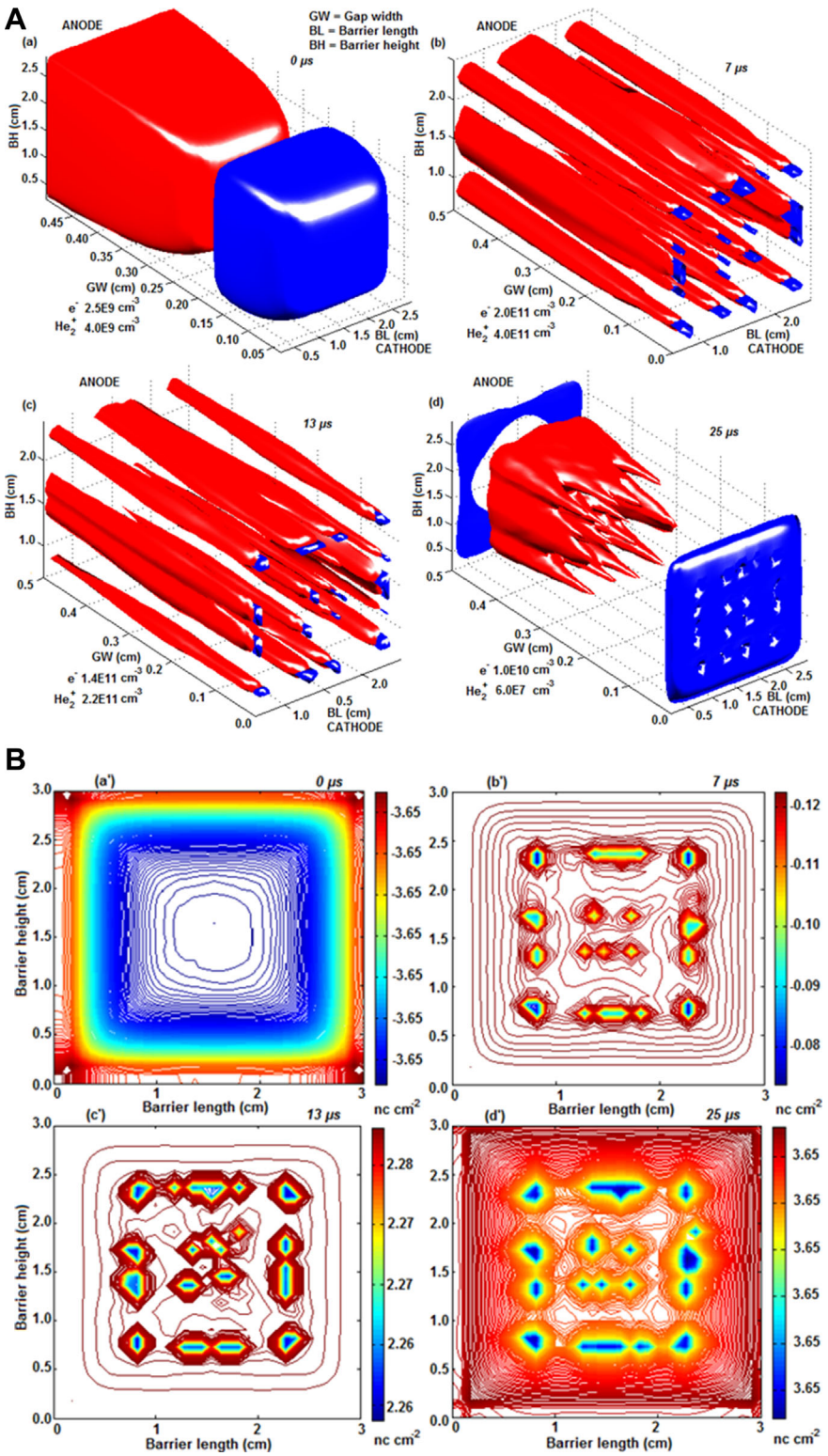

Figure 2. (a–d) Iso-contours of electron (red) and molecular helium ion (blue) density (left), and (a′–d′) slice distribution of surface charge density (right) in the case of four different time instants (0, 7, 13, and 25 μs) during the evolution of the negative discharge current pulse at $f = 10$ kHz, $V_o = -1.7$ kV, $\epsilon_r = 9.0$, BW = 0.25 cm, and 50 ppm N_2 impurities.

© 2015 WILEY-VCH Verlag GmbH & Co. KGaA, Weinheim

Early View Publication; these are NOT the final page numbers, use DOI for citation !!

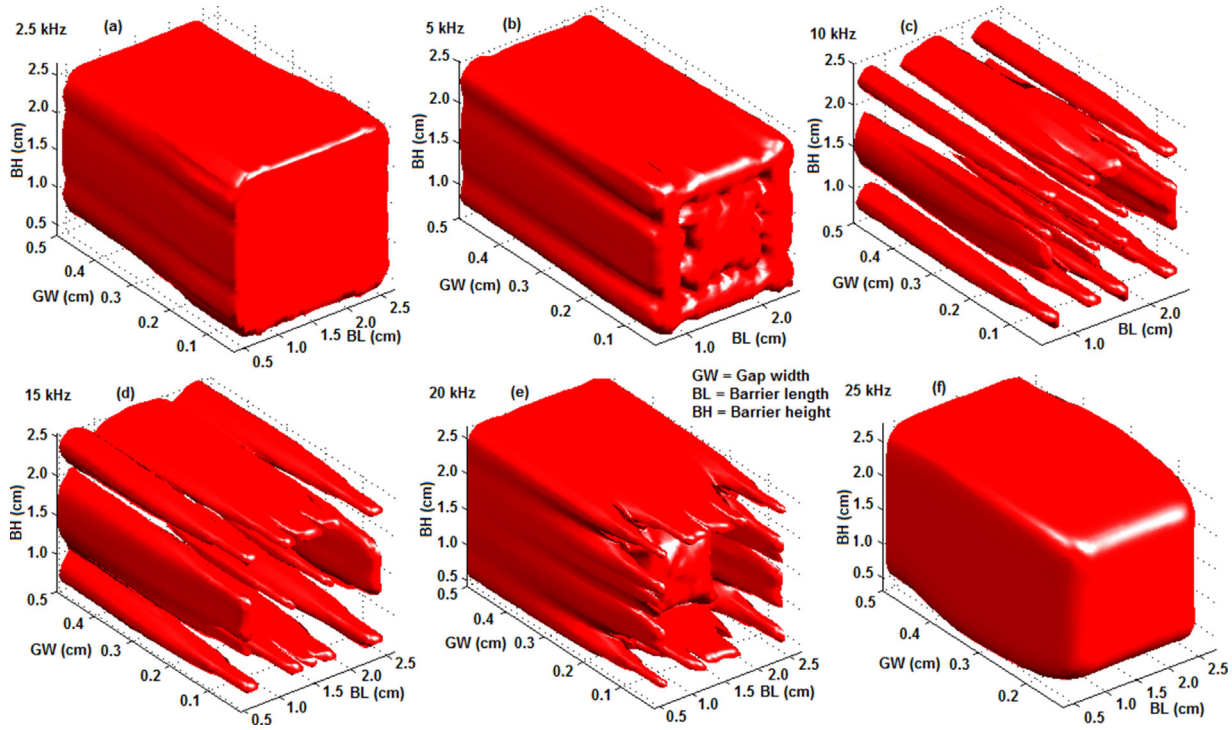

Figure 3. Volumetric profiles of electron density in the filamentary DBD plasma at the maximum value of the negative discharge current density using (a) 2.5 kHz, (b) 5 kHz, (c) 10 kHz, (d) 15 kHz, (e) 20 kHz, and (f) 25 kHz, $V_o = -1.7$ kV, $\epsilon_r = 9.0$, BW = 0.25 cm, and 50 ppm N_2 impurities.

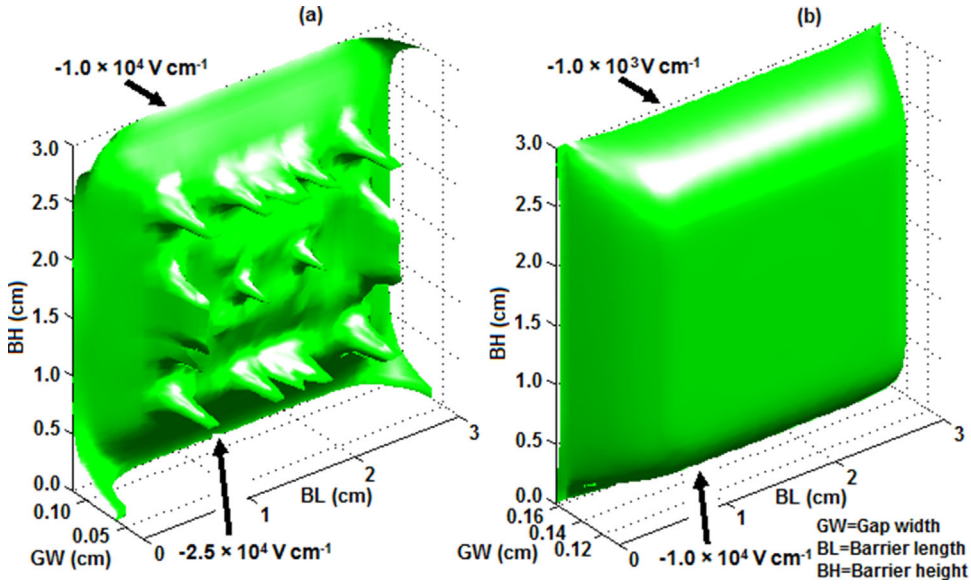

Figure 4. Volumetric profiles of axial electric field (E_y) at the maximum value of the negative discharge current density using (a) $V_o = -1.7$ kV and (b) $V_o = -1.5$ kV at $f = 15$ kHz, $\epsilon_r = 9.0$, BW = 0.25 cm, and 50 ppm N_2 impurities.

© 2015 WILEY-VCH Verlag GmbH & Co. KGaA, Weinheim
DOI: 10.1002/ppap.201400231

↖ Early View Publication; these are NOT the final page numbers, use DOI for citation !!

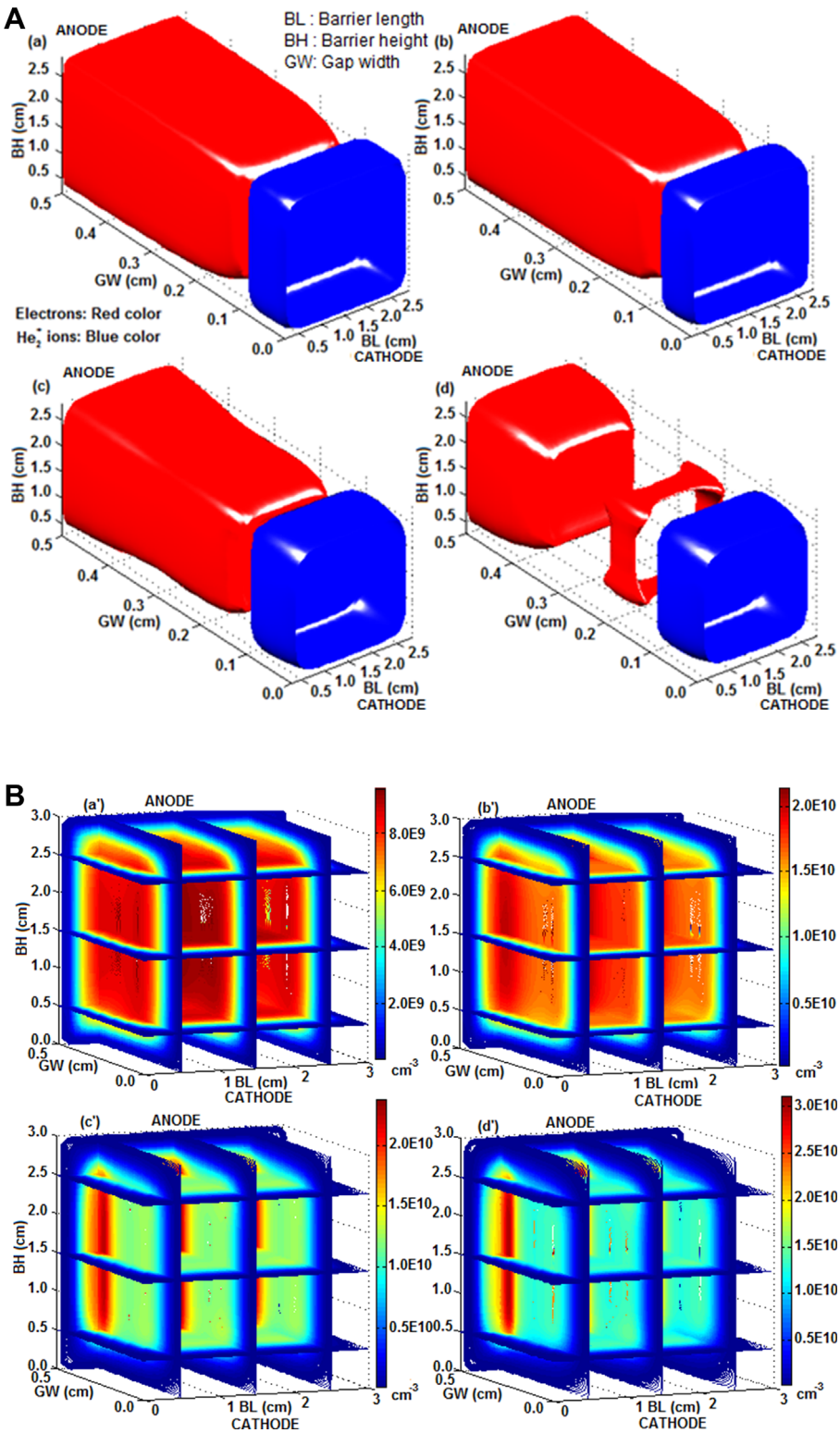

Figure 5. (a–d) Iso-contours of electrons (red) and He_2^+ ions (blue) density (left), and (a′–d′) slice distributions of electron density at different locations (right) in the bulk DBD plasma at the maximum value of the negative discharge current density using $f = 30$, 50, 70, and 90 kHz, $V_o = -1.5$ kV, $\epsilon_r = 7.5$, BW = 0.1 cm, and 20 ppm N_2 impurities.

© 2015 WILEY-VCH Verlag GmbH & Co. KGaA, Weinheim

Early View Publication; these are NOT the final page numbers, use DOI for citation !!

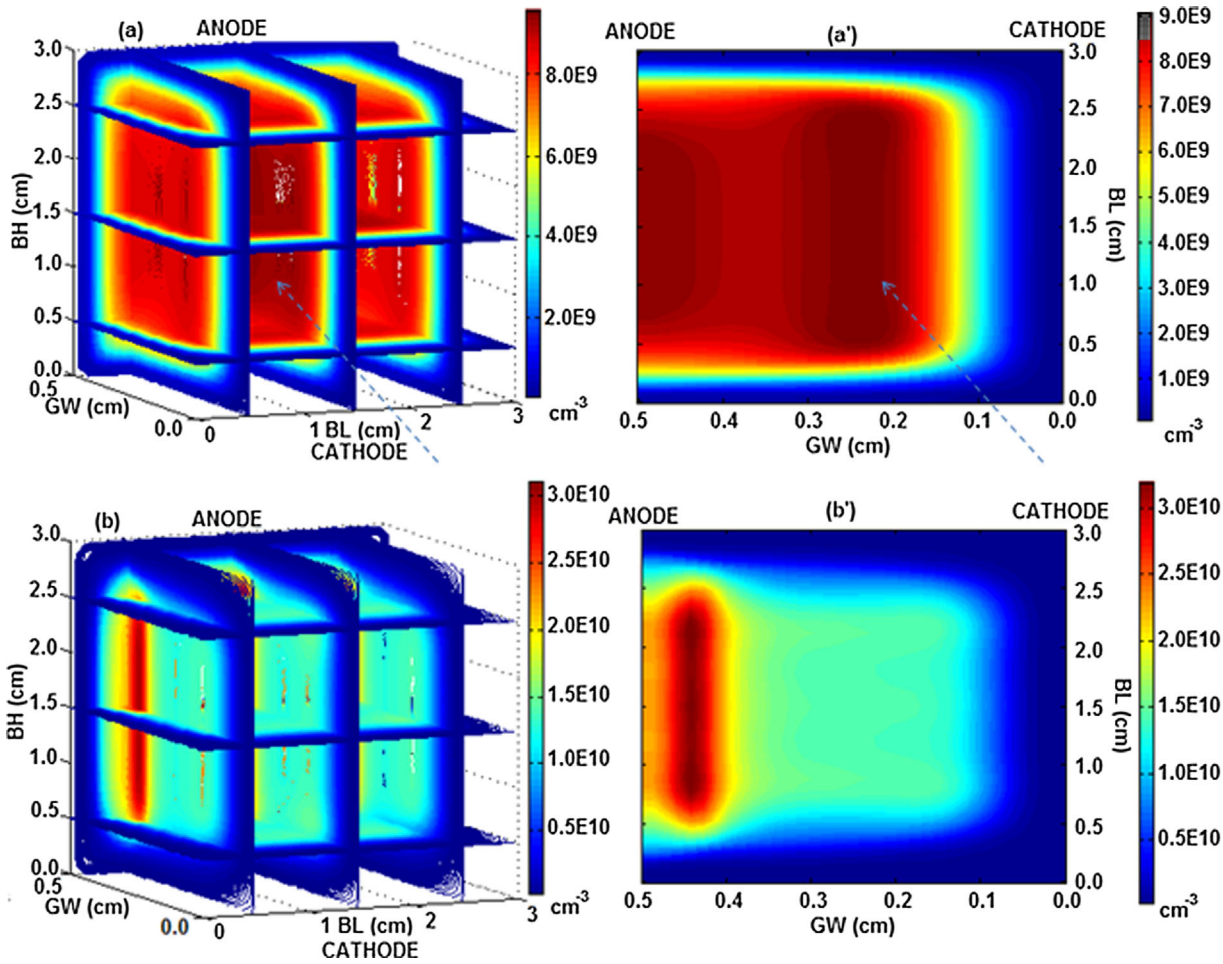

Figure 6. Comparison of (a, b) three-dimensional and (a′, b′) two-dimensional spatial slice distributions of electron density at the maximum value of the negative discharge current density using $f = 30$ and 90 kHz, $V_o = -1.5$ kV, $\epsilon_r = 7.5$, BW = 0.1 cm, and 20 ppm N_2 impurities.

three-dimensional space with a time constant ($\Delta t/3$) along the x, y, and z axes, respectively.

3. Results and Discussion

In this investigation, the development of a three-dimensional fluid model is essentially required to explore the volumetric expansion of filamentary and uniform atmospheric pressure DBD plasma using the parallel plate DBD reactor. For small gap spacing as 0.5 cm, the precise shape of filaments is not clear using two-dimensional fluid models; however, this can only be addressed by the application of three-dimensional fluid model to explain the volumetric behavior of the filaments. Here, the numerical simulation outcomes are used to express the behavior of filamentation under the specific operating conditions, such as small magnitude of overvoltage and driving frequency (f). We explain the behavior of driving frequency distributed into two lower and higher domains. The lower domain has a range from 2.5 to 25 kHz while the second domain exists in the range from 30 to 90 kHz. The characteristics of atmospheric pressure discharge plasma are modified when shifting from the lower to higher domains under input operating similar conditions instead of driving frequency. It is seen from the three-dimensional profiles of electron density that the filamentation is suppressed by the merging of filaments, specifically at 2.5 and 25 kHz under the application of overvoltage while appearing at specific frequencies of 5, 10, 15, and 20 kHz. In the second domain of frequency, the peak of electron density in the negative glow (NG) region at 30 kHz is entirely displaced near the anode barrier at 90 kHz, which indicates the dominant effect of frequency for the structure of uniform DBD plasmas.

In order to explore the behavior of filamentation, the magnitude of applied potential must be greater than the breakdown potential of a particular gas mixture and the

© 2015 WILEY-VCH Verlag GmbH & Co. KGaA, Weinheim

Early View Publication; these are NOT the final page numbers, use DOI for citation !!

residue between the imposed and breakdown potential is termed as overvoltage. The breakdown voltage is defined as the critical value at which the strong current starts flowing in the parallel plate DBD reactor and it is dependent on several parameters as discussed in refs.[10,12,21,23] If the value of residue is enhanced from 15 to 20% of threshold breakdown potential, the filamentation possibly prevails in discharge plasma at atmospheric pressure. The current simulation study contrasts the behavior of filamentation and uniformity under specific values of external imposed potentials, such as 1.7 and 1.5 kV for two different cases. To analyze the effect of overvoltage in DBD plasma in the first case, the amplitude of external imposed voltage is higher by 0.20 kV than the uniform discharge plasma case in He-N_2 gas and outcomes in the creation of constricted filamentary discharge. For this, the stationary state of DBD plasma is presented by the spatio-temporal iso-contours of the electron and He_2^+ ion density as well as SCD that reflect the condition of the powered cathodic dielectric barrier facing discharge plasma at four time instants, 0, 7, 13, and 25 μs during the evolution of negative discharge current pulse. The state of discharge plasma is categorized into three major domains during these mentioned time instants, such as pre-breakdown (0 μs), streamer breakdown (7 μs), and afterglow phase (13 and 25 μs) occurring in every half cycle of the discharge current pulse.

In pre-breakdown phase at 0 μs, the kinetics of electrons dominate in the large portion of reactor gap as compared to ions near the cathode barrier because of accumulation of negative charge on the surface of dielectric barrier, corresponding to the memory effect of preceding discharge current pulse as shown in Figure 2(a, a′). The bulk of DBD plasma represents the uniform structure of charge carriers in the pre-breakdown phase with small density of electrons 2.5×10^9 cm^{-3} and ions 4.0×10^9 cm^{-3}, approximately. The filamentation has not emerged at 0 μs because the breakdown does not occur at this stage. It is clear from the volumetric profiles of species density that the birth of an electron avalanche is initiated in the middle of gap as shown in Figure 2(a) and moves toward the cathode barrier from 0 to 7 μs. The secondary electrons eject from the surface of the cathode barrier by the ion bombardment in the breakdown phase, which are accelerated in the cathode fall layer (CFL) due to the strong push of mean electric field enhancing further ionization activities. When the breakdown proceeds further, the uniform structure of DBD plasma is entirely destroyed and the conducting channels of electron are developed as shown in Figure 2(b). These non-uniform channels are usually called filaments. While the Townsend breakdown mechanism is responsible for the creation of uniform discharge, the filaments clearly illustrate that the streamer breakdown is effective in the current scenario because of growing up of small conducting streams of electrons.

In the breakdown phase, the streamers develop in DBD plasma due to space charge created by the electron avalanche under the consequence of external imposed potential. The impedance of dielectric barrier is reduced sharply, which results in a large current by neutralizing the previously stored surface charges. This process occurs at a very rapid rate and the SCD approaches to 0 approximately at the peak of conduction discharge current density as shown in Figure 2(b′). The value of breakdown voltage is smaller than 1.7 kV in this case and its approximate value is 1.427 kV. Due to a large impulse of multiple ionization processes at different rates, the electron avalanche drifts rapidly and provides localized conducting channels in the bulk plasma. This kind of localization is categorized as strong and weak filaments appearing at different locations. To identify the mechanism for the independent existence of filaments, a confinement potential between any pair of adjacent filaments is evaluated by using Coulomb's repulsive and Lorentz attractive forces. It is found from the filamentary profiles of electron density that the Coulomb's repulsive force is much greater than the Lorentz attractive force that supports the independent existence of filaments and this approach is consistent with the previous modeling results as explained in ref.[35] The growth of filaments is directed from the anode toward the cathode barrier because the maximum concentration of electron shifts from middle of gap toward the NG region of filamentary discharge plasma. The electrons and ions acquire the maximum values of 2.0×10^{11} and 4.0×10^{11} cm^{-3} at this stage.

In the decay phase from 7 to 13 μs, the mean electric field weakens in the CFL and the density values diminish from the preceding time instant as shown in Figure 2(c). This happens due to quenching of electron production by the substantial energy losses. This behavior is entirely different from the uniform glow discharge plasma in which the electron density continuously increases until it reaches at the position of the new cathode fall layer.[14] The conducting channels in discharge plasmas are further constricted in space resulting in an increase of the impedance of dielectric barriers. So, the positive SCD increases during this phase as exhibited in Figure 2(c′). The densities of charge carriers diminish to 1.4×10^{11} and 2.2×10^9 cm^{-3} at 13 μs. In a normal uniform glow discharge, the electron density is steadily enhanced until its peak approaches at the position of the coming CFL of the half cycle. This situation is different in which the electron density starts falling after acquiring a peak value at 7 μs because of the impact of higher RC of N_2^+ ions. The discharge current pulse is not entirely symmetric in the present filamentary discharge plasma in which the amplitude of the negative discharge current pulse is stronger than positive discharge current pulse, but the primary aspects of discharge current density remain

© 2015 WILEY-VCH Verlag GmbH & Co. KGaA, Weinheim

Early View Publication; these are NOT the final page numbers, use DOI for citation !!

similar from one cycle to another after acquiring a stationary state.

The function of the enhanced value of the RC suppresses the value of electron density after 7 μs and the electron density consistently falls after this value as shown in Figure 2(c, c′). The increment in electron density from 0 to 7 μs is 100 times, which shows the immediate evolution of discharge plasma in the breakdown phase and it continuously falls after this value at 13 and 25 μs. In the afterglow phase, the positive SCD continuously increases on the dielectric barrier and the axial contraction of filaments in the bulk of the discharge plasma transforms the filaments into small spikes before the entire extinguishing of instability as shown in Figure 2(d, d′). This shows that the SCD acquires its peak value before the polarity reversal of external imposed potential at 25 μs. It is quite clear from Figure 2(d) that the ions are present near the peripheral edges of the new momentary cathode, which corresponds to the polarity reversal of external imposed potential. The density of electrons is reduced to the smallest possible value in the pre-ionization phase; however, the density of ions obtains its minimum possible value of 6.0×10^7 cm^{-3} at the fourth instant of time. Therefore, the spatial distribution of SCD provides a clear indication that the filaments have a substantial impact on the surface of the dielectric barrier facing discharge plasma during the evolution of negative discharge current pulse.

In order to explore the behavior of filamentation at other frequencies, we contrast the volumetric distribution of electron density at various driving frequencies as illustrated in Figure 3. The values of electron density are collected at the peak of discharge current density, which are shown in Table 1. In case of 2.5 kHz, the streamer breakdown has emerged as the dominant mechanism and ultimately produces a significant flow of charge carriers because of a greater time period of a cycle than other considered higher frequencies (5 to 25 kHz). The streamers grow rapidly in DBD plasma and this can be seen from the volumetric profile of electrons, which represents the entire merging of filaments at 2.5 kHz and partial merging at 5 kHz as indicated in Figure 3(a, b). The merging of filaments is more pronounced at 2.5 kHz than 5.0 kHz due to dominant effect of overvoltage. The expansion of filamentary channels becomes enormous at 2.5 kHz because of the longer time period in the breakdown phase. This comparison provides a clear direction of amplifying filamentation at 10 kHz, which can be verified from the filamentary contours of electron density as exhibited in Figure 3(c).

Subsequently, the breakdown phase is shortened at higher frequencies ($\leq$20 kHz) and caps the entire merging of filaments because of the extinguishing of growth of electron density and spatial spread of filaments at 15 and 20 kHz in three-dimensional space as shown in Figure 3 (d, e). It is seen from the numerical simulations that the immediate creation of filaments depends on the direct and Penning ionization processes in this phase. Since the impurities perform a major role in the atmospheric pressure discharges as described in ref.,[23] the current He-N_2 gas mixture involves small amount of nitrogen impurities. The Penning ionization mechanism has been recognized as extremely important in the breakdown phase. The filamentary structure of DBD plasma transforms into a uniform structure if the rate coefficient of Penning ionization is assumed as 0 instead of other chemical reactions in Table 2 mentioned in ref.[28] in the concerned frequency domain (2.5–25 kHz). This clearly indicates that the influence of nitrogen impurities performs a substantial role to modify the structure of DBD plasma in the breakdown phase and it occurs through an assertive contribution of Penning ionization than other ionization processes involving nitrogen impurities. The development of filamentation is also linked to the competition between these ionization rates in the He-N_2 gas mixture during the breakdown phase. This means that the Penning ionization operates as a destructive agent for the metastables and creates a suitable environment for the formation of filamentation in discharge plasma. So, the proper control of the annihilation of metastables can be achieved by the addition of varying amounts of nitrogen into the helium gas, which ultimately results in the form of filamentary or uniform discharge plasma due to the dominance of Penning ionization.

Figure 3(c) shows the sharp filamentation in the structure of electron density at 10 kHz relative to other frequencies and the literature discussed the characteristic features

Table 2. Maximum values of species density and magnitude of discharge current density at $V_o = -1.5$ kV, $\epsilon_r = 7.5$, and 20 ppm N_2 impurities.

Driving frequency [kHz]	Electron density [cm^{-3}] $\times 10^{10}$	He_2^+ ion density [cm^{-3}] $\times 10^{10}$	Conduction discharge current density [mA cm^{-2}]
30	0.92	2.10	1.35
50	2.10	4.10	2.30
70	2.40	4.75	1.85
90	3.10	5.40	1.70

© 2015 WILEY-VCH Verlag GmbH & Co. KGaA, Weinheim

↖ Early View Publication; these are NOT the final page numbers, use DOI for citation !!

of filamentation in plasma under various conditions.[14,17,21,34] At 15 kHz, the filamentary behavior starts being suppressed as shown in Figure 3(d) and it further quashed at 20 kHz and completely stopped at 25 kHz under similar assumptions as illustrated in Figure 3(e, f). The fusion of filaments at 25 kHz is due to the short time period of the cycle because of the controlling of growth and it can be verified with a decrease in the electron and ion densities as displayed in Table 1. This presents a clear evidence that the streamer breakdown is shifted into the Townsend breakdown by increasing of driving frequency. The Townsend breakdown mechanism becomes dominant when the frequency is increased further after the limit (>25 kHz) because of the coalescence of filaments. The filamentary or non-uniform discharge mode is extinguished at lower frequencies (<7 kHz) by the merging of filaments due to the longer time period of oscillating cycle and it actively emerges in the intermediate range (8–20 kHz) and again effectively transforms into a uniform mode at higher frequencies (>20 kHz) due to the contracting of the time period under similar imposed conditions. Thus, the evolution of uniform glow discharge plasma can be controlled by the application of driving frequency in DBD plasmas.

To characterize the significance of overvoltage, the filamentary and uniform profiles of axial electric field (E_y) are distinguished at the maximum value of discharge current density under different magnitudes of external imposed potentials, such as −1.7 and −1.5 kV as shown in Figure 4. The streamer breakdown mechanism does not evolve in the case of −1.5 kV because the value of overvoltage is not significantly higher to initiate an intense breakdown in the gas mixture, which is essential for the birth of streamers. The initial distribution of electron density and electron mean energy are similar in both cases to exclude the artificial effects for the development of filamentation.

To figure out the origin of filamentary and uniform discharge plasma, the electric field created by the breakdown of dielectric barrier is compared at the maximum value of discharge current density during the negative discharge current pulse. In the breakdown phase, the electric field enhances strongly by the rapid growth of electron avalanche, although, the conflicting electric field from the dielectric barrier due to build-up of surface charge makes it possible to stabilize the atmospheric pressure discharge plasma in uniform and filamentary discharge modes. For this purpose, we contrast the values of the axial electric field along the constricted tips than the uniform plasma as clearly seen in Figure 4(a, b). The non-uniform profile of electric field indicates that the peaks of electron and ion density are established near the cathode barrier along the filaments, which verifies with the greater strength of electric field than the surroundings of DBD plasma. When the value of overvoltage (0.2 kV) is lowered to 0, the mechanism of streamer breakdown shifts into Townsend breakdown as precisely represented in the contrasting profiles of electric field in Figure 4. This shows that the electric field ($-2.5 \times 10^4\,\mathrm{V\,cm^{-1}}$) in the constricted part is significantly greater than the other parts ($-1.0 \times 10^4\,\mathrm{V\,cm^{-1}}$) on the surface of dielectric barrier, while it becomes uniform for the glow discharge plasma near the barrier surface as shown in Figure 4(a, b). Due to non-uniform distribution along the surface of dielectric barrier, the filamentary discharge plasma cannot be regarded as a viable source for the sophisticated industrial and medical applications, such as surface coatings and wound treatment as compared to the uniform atmospheric pressure glow discharge plasma. The magnitude of electric field is changed from 2.5×10^4 to $1.0 \times 10^4\,\mathrm{V\,cm^{-1}}$ in the filamentary discharge plasma, while it is altered from 1.0×10^4 to $1.0 \times 10^3\,\mathrm{V\,cm^{-1}}$ in the case of uniform discharge plasma.

When the driving frequency is increased under the above-mentioned similar operating conditions, a Townsend mode of discharge plasma appears rather than uniform glow discharge plasma. The weak Townsend mode of discharge plasma evolves by the destruction of metastables through the Penning ionization process. In order to explore the major contribution of driving frequency for the trapping of electrons in the breakdown phase, we reduce the trace amount of nitrogen impurities from 50 to 20 ppm to balance the destruction metastables in the specified domain of frequency (30 to 90 kHz) and also reduces the permittivity of dielectric barrier to control the uniformity of discharge plasma. In this way, it is possible to distinguish the trapping mechanism of electrons in the breakdown phase as well as a uniform glow atmospheric pressure DBD plasma using 20 ppm nitrogen impurities. When the stationary state is obtained in the second domain of frequency, the positive and negative discharge current pulses are approximately in symmetric form.

For expressing the deviation in the behavior of uniformity at higher frequencies, the volumetric density profiles of electrons and He_2^+ ions are presented at the peak of the conduction discharge current density at four specific frequencies (30, 50, 70, and 90 kHz) as shown in Figure 5(a–d). When the breakdown of gas mixture occurs in DBD reactor, the charge particles move rapidly toward their respective cathode and anode barriers. Subsequently, the distorted profile of molecular helium ions is formed near the cathode barrier along with small peak of electrons in the NG region, which qualifies as the reliable criteria of uniform glow discharge plasma[8–10,14,21,23] with four specific regions, such as CFL, NG, Faradays dark space (FDS), and Positive column (PC). These regions are clearly identified at

© 2015 WILEY-VCH Verlag GmbH & Co. KGaA, Weinheim

Early View Publication; these are NOT the final page numbers, use DOI for citation !!

30 kHz as exhibited in Figure 5(a, a′), which show that the uniform glow discharge plasma exists and it modifies after amplifying frequency. At 50 kHz, these regions are slightly updated in three-dimensional space because the peak of electron density is displaced toward the anode barrier and weakens the distorted profile of molecular helium ions as shown in Figure 5(b, b′). This changes the structure of glow discharge in the category of partial uniform glow discharge plasma at 50 kHz.

As the frequency is further incremented to 70 kHz, the entire structures of electron and ion are modified in discharge plasma. It is observed from the density profile of He_2^+ ions that the distortion further reduces near the cathode barrier with spatial expansion, and the peak of electrons is shifted near the anode barrier as distinctly contrasted from the volumetric profiles and slice distributions at different locations in the bulk of the DBD plasma in Figure 5(c, c′). This elucidates that the uniform structure at 30 kHz is continuously modified by the influence of oscillating frequency, which can be compared in the distributions of electron and ion densities. Eventually, the peak of electron density is further compressed with a wider spread of ions near the cathode barrier at 90 kHz as exhibited in Figure 5(d, d′). It is evident from Table 2 that the density values of electron and He_2^+ ion are continuously enhancing with frequency, but the uniform structure of glow discharge plasma is a variant from 30 to 90 kHz. As we know that the emitted electrons from the multiple sources (imposed potential and secondary emission) gain energy from the mean electric field of the CFL in discharge plasma, which are also altered by the significance of frequency. This means that when the polarity of external imposed potential is quickly flipped after this frequency limit (>50 kHz), the flow of electrons and ions in the gap cannot maintain a uniform structure to meet the criterion of four specific parts. In this frequency regime, the internal kinetic behavior of charge particles is so rapidly modulated, which reverses the direction of drift motion of charge carriers before reaching the dielectric barriers of opposite polarity. This caps the amplification in the conduction discharge current density after 50 kHz because the peaks of electrons and ions are moved away from the cathode barrier.

Correspondingly, the electrons are trapped in a narrow portion in the PC. These trapped electrons enhance the production rate of charged particles due to the collisions with gas atoms, but the source of secondary emission of electrons is adversely depressed because the ionic species reflect back from their path before hitting with the surface of the cathode barrier.[36] The creation of residual current density depends on the trapping of electrons, which is increased by a rise in frequency during the polarity reversal of discharge current pulse. If we measure the approximate width of electron density in the PC, it shrinks in space along the axial direction from 0.1 cm at 50 kHz to 0.05 cm at 90 kHz with an increase in the magnitude of density as displayed with the double-ended arrows in the slice distributions of electrons in Figure. 4 (b′–d′). The mentioned width in electron density is further curtailed after 90 kHz under similar conditions and we checked the similar pattern of squeezing of electron density before this limit (<150 kHz). This shows that the behavior of DBD plasma is consistently modified in the mentioned driving frequency regime as shown by a combination of slices in Figure. 4(a′–d′). Hence, these density profiles indicate that the uniform glow discharge is obtained in a specific domain of frequency at atmospheric pressure.

3.1. Comparison of Three-Dimensional and Two-Dimensional Fluid Models

To provide the reliability of numerical simulations, we compare the spatial slice distributions of electron density collected from the three-dimensional fluid model with previously developed two-dimensional fluid model described in detail[13,28] under similar input operating conditions, such as barrier length and width, gap spacing, dielectric constant, driving frequency, and external imposed potential. The numerical modeling outcomes of three and two-dimensional fluid models are compared when the temporal profiles of discharge current density remain the same from one cycle to another. In uniform atmospheric pressure DBD plasma, the peak of electron density is observed clearly in the negative glow region at 30 kHz as represented with arrows in Figure 6(a, a′), while the location of this density peak is shifted into the positive column near the anode barrier at 90 kHz as shown in Figure 6(b, b′). The above-mentioned four regions (CFL, NG, FDS, and PC) existing in the uniform glow discharge are exactly identified at 30 kHz using both fluid models. It is evident from the slice distributions of electron density at 30 and 90 kHz that their maximum numerical values ($\sim 0.91 \times 10^{10}$, $\sim 3.25 \times 10^{10}\,cm^{-3}$) are approximately similar in the case of three and two-dimensional fluid models. The behavior of coagulation of electrons near the anode barrier is identified at 90 kHz, which shows the resembling of numerical results obtained from three and two-dimensional fluid models as shown in Figure 6(b, b′). Moreover, the comparison of three and two-dimensional slice distributions of electron density illustrates that the outcomes of both models are in good agreement under similar working conditions. Thus, the above discussion indicates that the consequences of three-dimensional fluid model are reliable to describe the dynamic significance of charged particles during the breakdown phase of the atmospheric pressure DBD plasma.

© 2015 WILEY-VCH Verlag GmbH & Co. KGaA, Weinheim

↖ Early View Publication; these are NOT the final page numbers, use DOI for citation !!

4. Conclusion

In conclusion, the three-dimensional fluid model in this study provides a clear understanding of the filamentary and uniform distributions of atmospheric pressure DBD plasma under the influence of overvoltage and driving frequency. The spatial distributions of electron density illustrate that the behavior of filamentation in discharge plasma consistently modifies in the specific frequency domain (2.5 to 25 kHz) at atmospheric pressure. For uniform DBD plasma, a benchmark criterion of four distinct regions (CFL, NG, FDS, and PC) is recognized at 30 kHz, which is further modulated into partial uniform glow discharge plasma at higher frequencies ($\geq$50 kHz). Also, we have identified the contrasting profiles of electron and ion density at distinct frequencies (30, 50, 70, and 90 kHz), which showed that the density peak of electrons in the NG region at 30 kHz is shifted in the PC near the anode barrier at 90 kHz, and the distorted peak of He_2^+ ions at 30 kHz broadens near the cathode barrier at 90 kHz. This simulation study enhances an understanding of atmospheric pressure DBD under the impulse of driving frequency in two distinct domains. Finally, the results of three and two dimensional fluid models are compared to provide the correctness of numerical simulation results.

Acknowledgements: This work is supported by Science Foundation Ireland under grant 08/SRC/I1411. Special thanks to Dr. Paul Swift for the editing and nice suggestions during the preparation of this paper.

Received: December 5, 2014; Revised: March 24, 2015; Accepted: March 24, 2015;DOI: 10.1002/ppap.201400231

Keywords: atmospheric pressure discharges; dielectric barrier discharge; filamentation and Helium; nitrogen gas mixture; three-dimensional modeling; uniformity

[1] U. Kogelschartz, B. Eliasson, W. Egli, *Pure Appl. Chem.* **1999**, *71*, 1819.
[2] S. Okazaki, M. Kogoma, *J. Photopolym. Sci. Technol.* **1993**, *6*, 339.
[3] J. Hong, S. Kim, K. Lee, K. Lee, J. J. Choi, Y.-K. Kim, *Proc. VIIIth Int. Symp. On High Pressure Low Temperature Plasma Chem.*, Puhajarve, Estonia, Vol. *2*, **2002**, pp. 360–363.
[4] S. Kanazawa, M. Kogoma, T. Moriwaki, S. Okazaki, *J. Phys. D: Appl. Phys.* **1988**, *21*, 838.
[5] T. Yokoyama, M. Kogoma, S. Kanazawa, T. Moriwaki, S. Okazaki, *J. Phys. D: Appl. Phys* **1990**, *23*, 374.
[6] B. Eliasson, U. Kogelschatz, *IEEE Trans. Plasma Sci.* **1991**, *19*, 1063–1077.
[7] A. Fridman, *Plasma Chemistry*, Vol. *83*, Cambridge University Press, New York **1998**.
[8] F. Massines, A. Rabehi, Ph. Decomps, R. B. Gadri, P. Segur, C. Mayoux, *J. Appl. Phys.* **1998**, *83*, 2950.
[9] Yu. B. Golubovskii, V. A. Mairov, J. Behnke, J. F. Behnke, *J. Phys. D: Appl. Phys.* **2003**, *36*, 39.
[10] L. Mangolini, C. Anderson, J. Heberlein, U. Kortshagen, *J. Phys. D: Appl. Phys.* **2004**, *37*, 1021.
[11] G. Nersisyan, W. G. Graham, *Plasma Sources Sci. Technol.* **2004**, *13*, 582–587.
[12] F. Tochikubo, T. Chiba, T. Watanabe, *Jpn. J. Appl. Phys.* **1999**, *38*, 5244.
[13] M. M. Iqbal, M. M. Turner, *Contrib. Plasma Phys.* **2014**, *54*, 756.
[14] P. Zhang, U. Kortshagen, *J. Phys. D: Appl. Phys.* **2006**, *39*, 153.
[15] D. Braun, V. Gibalovt, G. Pietsch, *Plasma Sources Sci. Technol.* **1992**, *7*, 166.
[16] M. Meyyappan (Ed.), *Computational Modeling in Semiconductor Processing*, Artech House, Inc., Norwood, MA **1995**.
[17] A. A. Kulikovsky, *Phys. Lett. A* **1998**, *245*, 445.
[18] L. Stollenwerk, Sh. Amiranashvili, J.-P. Boeuf, H.-G. Purwins, *Phys. Rev. Lett* **2006**, *96*, 255001.
[19] Chao Li, Ute Ebert, Willem Hundsdorfer, *J. Comp. Phys.* **2012**, *231*, 1020.
[20] A. Luque, U. Ebert, *J. Comp. Phys.* **2012**, *231*, 904.
[21] Y. P. Raizer, *Gas Discharge Physics*, Springer-Verlag, Berlin **1991**.
[22] T. Callegari, B. Bernecker, J. P. Boeuf, *Plasma Sources Sci. Technol.* **2014**, *23*, 054003.
[23] Y. Wang, D. Wang, *Phys. Plasmas.* **2005**, *12*, 023503.
[24] G. J. M. Hagelaar, Ph.D Thesis, Technische Universiteit Eindhoven, 2000.
[25] D. P. Lymberopoulos, D. J. Economou, *J. Vac. Sci. Technol. A* **1994**, *12*, 1229.
[26] G. J. M. Hagelaar, L. C. Pitchford, *Plasma Sources Sci. Technol.* **2005**, *14*, 722.
[27] M. Brunger, S. J. Buckman, L. J. Allen, *J. Phys. B: At. Mol. Opt. Phys.* **1992**, *25*, 1823.
[28] M. M. Iqbal, Ph.D Thesis, School of Physical Sciences, Dublin City University, Ireland, 2010.
[29] P. J. Roache, *Computational Fluid Dynamics*, Hermosa, Albuquerque, NM **1976**.
[30] D. L. Scharfetter, H. K. Gummel, *IEEE Trans. Electron Devices* **1969**, *16*, 64.
[31] H. L. Stone, *SIAM J. Numer. Anal.* **1968**, *5*, 530.
[32] M. Zedan, G. E. Schneider, *AIAA J.* **1983**, *21*, 295.
[33] L. A. Stephen, *Physical Rev. D* **1981**, *23*, 2901.
[34] D. W. Peaceman, H. H. Rachford, Jr., *J. Soc. Indust. Appl. Math.* **1955**, *3*, 28.
[35] T. Shirafuji, T Kitagawa, T. Wakai, K. Tachibana, *Appl. Phys. Lett.* **2003**, *83*, 2309.
[36] A. M. Howatson, *An Introduction to Gas Discharges*, Pergamon Press, University of Michigan, New York **1976**.

© 2015 WILEY-VCH Verlag GmbH & Co. KGaA, Weinheim

Early View Publication; these are NOT the final page numbers, use DOI for citation !!